Article

Cell Stem Cell

MSC-Regulated MicroRNAs Converge on the Transcription Factor FOXP2 and Promote Breast Cancer Metastasis

Graphical Abstract

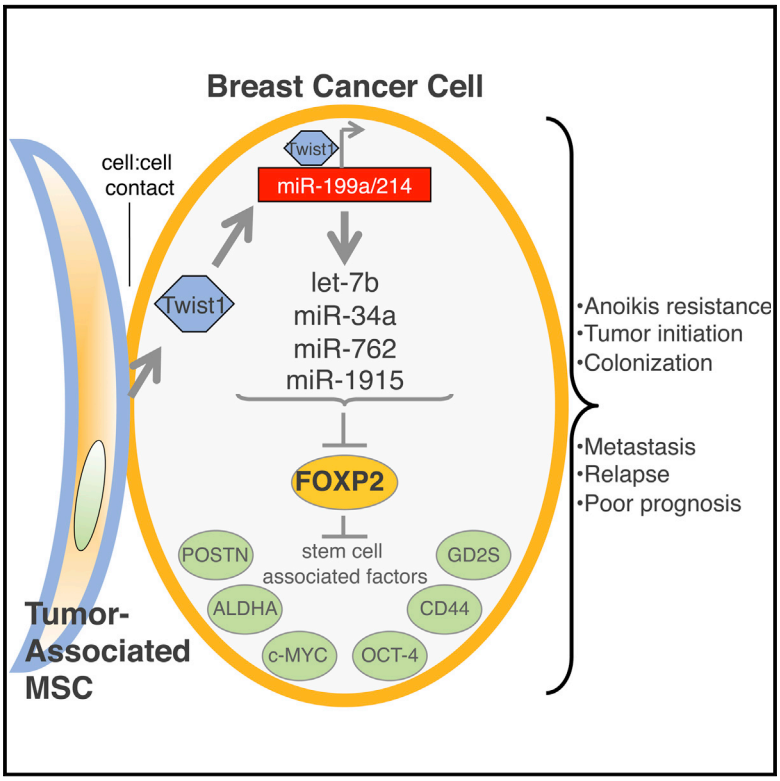

Highlights

MSCs promote contact-dependent upregulation of miR-199a in breast cancer cells

MiR-199a represses the transcriptional regulator FOXP2

The miR-199a-FOXP2 axis propagates cancer stem cell traits and metastasis

Elevated miR-199a and depleted *FOXP2* characterize malignant clinical breast cancer

Authors

Benjamin G. Cuiffo, Antoine Campagne, ..., Daniela Taverna, Antoine E. Karnoub

Correspondence

akarnoub@bidmc.harvard.edu

In Brief

Cuiffo et al. show that repression of the speech-associated gene *FOXP2* by a network of mesenchymal-stem-cell-regulated microRNAs facilitates the acquisition of cancer stem cell and metastatic phenotypes by breast cancer cells.

Cuiffo et al., 2014, Cell Stem Cell 15, 762–774
December 4, 2014
http://dx.doi.org/10.1016/j.stem.2014.10.001

CellPress

CellPress

Cell Stem Cell
Article

MSC-Regulated MicroRNAs Converge on the Transcription Factor FOXP2 and Promote Breast Cancer Metastasis

Benjamin G. Cuiffo,[1] Antoine Campagne,[1,2] George W. Bell,[3] Antonio Lembo,[4] Francesca Orso,[4] Evan C. Lien,[1] Manoj K. Bhasin,[5] Monica Raimo,[4] Summer E. Hanson,[6] Andriy Marusyk,[7] Dorraya El-Ashry,[8] Peiman Hematti,[6] Kornelia Polyak,[7] Fatima Mechta-Grigoriou,[2] Odette Mariani,[2] Stefano Volinia,[9] Anne Vincent-Salomon,[2] Daniela Taverna,[4] and Antoine E. Karnoub[1,10,11,*]

[1]Department of Pathology, Beth Israel Deaconess Medical Center, Harvard Medical School, Boston, MA 02215, USA
[2]Institut Curie, 75248 Paris Cedex 05, France
[3]Whitehead Institute for Biomedical Research, Cambridge, MA 02142, USA
[4]Department of Molecular Biotechnology and Health Sciences, University of Turin and MBC, 10126 Torino, Italy
[5]Department of Medicine, Beth Israel Deaconess Medical Center, Harvard Medical School, Boston, MA 02215, USA
[6]Carbone Cancer Center, University of Wisconsin-Madison, School of Medicine and Public Health, Madison, WI 53792, USA
[7]Department of Medical Oncology, Dana-Farber Cancer Institute, and Department of Medicine, Harvard Medical School, Boston, MA 02115, USA
[8]Department of Medicine, Sylvester Comprehensive Cancer Center, University of Miami Miller School of Medicine, Miami, FL 33136, USA
[9]Department of Morphology, Surgery and Experimental Medicine, Human Anatomy Branch, University of Ferrara, 44121 Ferrara, Italy
[10]Harvard Stem Cell Institute, Cambridge, MA 02138, USA
[11]Broad Institute of MIT and Harvard, Cambridge, MA 02142, USA
*Correspondence: akarnoub@bidmc.harvard.edu
http://dx.doi.org/10.1016/j.stem.2014.10.001

SUMMARY

Mesenchymal stem/stromal cells (MSCs) are progenitor cells shown to participate in breast tumor stroma formation and to promote metastasis. Despite expanding knowledge of their contributions to breast malignancy, the underlying molecular responses of breast cancer cells (BCCs) to MSC influences remain incompletely understood. Here, we show that MSCs cause aberrant expression of microRNAs, which, led by microRNA-199a, provide BCCs with enhanced cancer stem cell (CSC) properties. We demonstrate that such MSC-deregulated microRNAs constitute a network that converges on and represses the expression of *FOXP2*, a forkhead transcription factor tightly associated with speech and language development. FOXP2 knockdown in BCCs was sufficient in promoting CSC propagation, tumor initiation, and metastasis. Importantly, elevated microRNA-199a and depressed *FOXP2* expression levels are prominent features of malignant clinical breast cancer and are associated significantly with poor survival. Our results identify molecular determinants of cancer progression of potential utility in the prognosis and therapy of breast cancer.

INTRODUCTION

Cancer cells within breast carcinomas coexist with a heterogeneous milieu of stromal cells that collectively constitute the tumor-associated microenvironment. Numerous studies have provided substantial evidence that the interactions between cancer cells and components of the tumor stroma are pivotal in breast cancer pathogenesis (Barcellos-Hoff et al., 2013). In particular, such interactions—which co-opt mechanisms of wound healing, tissue maintenance, or development—appear to induce changes in cancer cells that are sufficient to actuate metastatic progression (Quail and Joyce, 2013). On this front, our group and others have shown that contextual mechanisms instigated in the cancer cells by the tumor microenvironment can cause dramatic increases in cancer malignancy via ostensibly reversible processes, such as epithelial-to-mesenchymal transitions (EMTs) (e.g., El-Haibi et al., 2012; Polyak and Weinberg, 2009). Indeed, cancer cells appear to be highly responsive to promalignant signals originating from the tumor microenvironment, providing attractive new avenues for the development of therapeutic approaches based on the inhibition of tumor-stroma crosstalk.

Mesenchymal stem cells (MSCs; also known as mesenchymal stromal cells) are a heterogeneous class of stromal progenitor cells that participate in tissue maintenance under normal homeostasis and are likewise closely associated with pathologic stromal responses to tissue injury and neoplasia (Cuiffo and Karnoub, 2012; Prockop et al., 2010). In the context of developing breast carcinomas, tumor-proximal MSCs have been shown to serve as active catalysts of cancer progression, robustly promoting breast cancer cell (BCC) invasion and metastasis (Karnoub et al., 2007; Goldstein et al., 2010; Liu et al., 2011; El-Haibi et al., 2012; Chaturvedi et al., 2013). MSCs have also been described to play similar roles in other cancer contexts, including lung cancer (Suzuki et al., 2011), prostate cancer (Prantl et al., 2010), and colon cancer (Shinagawa et al., 2010), suggestive of general promalignant activities for MSCs recruited into epithelial tumors. Indeed, MSCs recovered from human breast,

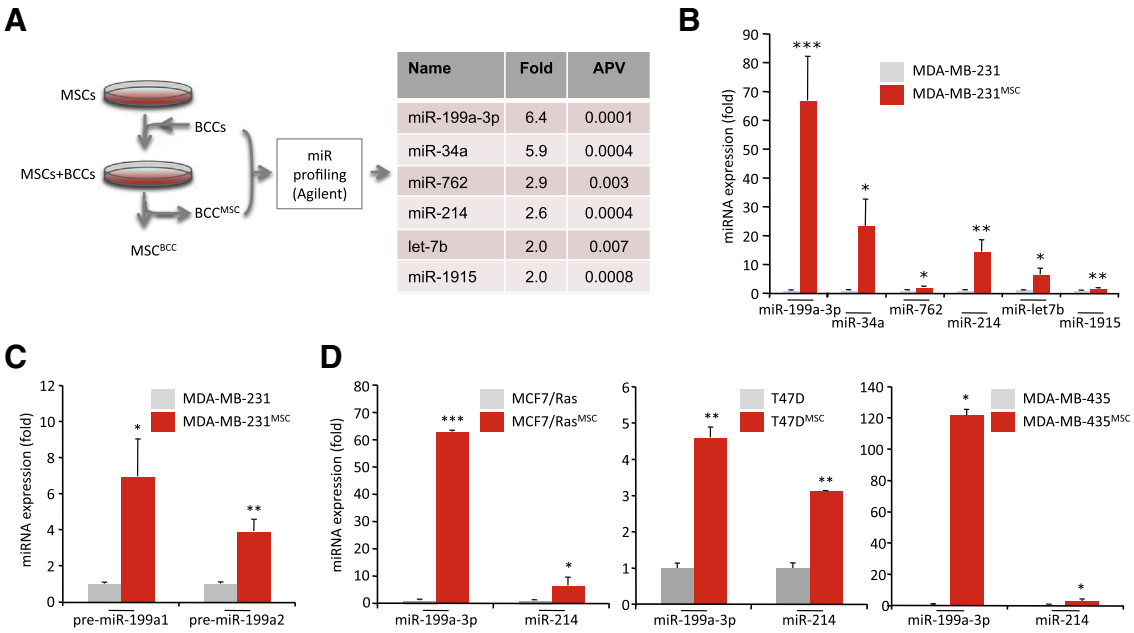

Name	Fold	APV
miR-199a-3p	6.4	0.0001
miR-34a	5.9	0.0004
miR-762	2.9	0.003
miR-214	2.6	0.0004
let-7b	2.0	0.007
miR-1915	2.0	0.0008

Figure 1. Induction of miR-199a and miR-214 in MSC-Primed BCCs

(A) Schematic of MSC+BCC coculture and sorting of BCCs for miRNA profiling. Six miRNAs were enriched ≥2.0-fold in MSC-activated BCCs (BCC^{MSC}) compared to resting BCCs (APV is adjusted p value, n = 4).

(B) Semiquantitative real-time PCR (rtPCR-ΔΔct) validation of the mature miRNAs identified in (A).

(C) rtPCR-ΔΔct probing precursor stem-loops derived from miR-199a1 and miR-199a2 (n = 3).

(D) rtPCR-ΔΔct probing miR-199a2-derived mature miRNAs in MSC-activated MCF7/Ras, T47D, and MDA-MB-435 cells; $MCF7/Ras^{MSC}$; $T47D^{MSC}$; and $MDA\text{-}MB\text{-}435^{MSC}$ (n = 3).

All rtPCR-ΔΔct panels display mean fold enrichment ± SEM. *p < 0.05; **p < 0.01, ***p < 0.001 in two-tailed Student's t test. See also Figure S1.

prostate, or ovarian tumors display promalignant phenotypes indicative of their crucial supportive functions in the progression of these tumors (McLean et al., 2011; Yan et al., 2012; Jung et al., 2013). However, at present, the molecular mechanisms underlying MSC contributions to tumor pathogenesis remain incompletely understood.

MicroRNAs (miRNAs, or miRs) are short noncoding RNAs that regulate gene expression via hybridization to complementary sequences of mRNAs, resulting in either translational inhibition or degradation of the target sequences (Bartel, 2009). miRNAs may affect the expression of hundreds of targets, thereby serving to define cellular identity and differentiation state through large-scale regulation of gene expression programs (Miyoshi et al., 2011). Importantly, miRNAs play critical functions in cancer pathogenesis and an expanding body of evidence has cataloged their deregulation in multiple aspects of tumor development, including invasion and metastasis (Ma et al., 2007; Tavazoie et al., 2008). To date, however, promalignant alterations to the cancer cell miRNA landscape as derived from their interactions with stromal cells have not been comprehensively characterized.

In the present work, we sought to identify potential miRNA deregulations associated with breast cancer malignancy instigated by prometastatic MSCs. We found that MSCs trigger a select set of miRNAs in BCCs, which, spearheaded by miR-199a, converge on and repress the expression of the transcription factor forkhead-box P2 (FOXP2). FOXP2 is a transcriptional repressor that has been primarily implicated in regulating speech and language development, as well as developmental neurogenesis, in humans (Fisher and Scharff, 2009; Tsui et al., 2013; Vernes et al., 2011). Aside from serving functions in the differentiation of tissues such as lung and esophagus (Shu et al., 2007), little is known regarding the roles of FOXP2 in nonneuronal contexts. We report here that miR-199a overexpression, or *FOXP2* silencing, endows BCCs with cancer-stem-cell (CSC)-like traits, enhances their tumor-initiating capabilities, and fosters their metastatic propensities. We describe miR-199a upregulation and *FOXP2* repression as prominent features of aggressive clinical breast cancers, and we found that they represent independent prognostic parameters for overall patient survival, indicative of their critical roles in breast tumor pathogenesis. Our work implicates a causal role for the speech gene *FOXP2* in breast cancer metastasis and elucidates elements of its tumor-stroma-initiated miRNA regulatory network.

RESULTS

MSC Priming Induces miR-199a-3p and miR-214 in BCCs

To characterize the miRNA alterations exhibited by MSC-primed BCCs, we cultured GFP-labeled MDA-MB-231 BCCs together with human bone-marrow-derived MSCs (BCC:MSC ratio of 1:3) for 3 days. GFP-BCCs were then isolated by fluorescence-activated cell sorting (FACS; $MDA\text{-}MB\text{-}231^{MSC}$), and their mature miRNAs were profiled by subtractive miRNA arrays (Agilent) using RNA derived from resting GFP-BCCs cultured alone as control (Figure 1A). These analyses revealed that only six

miRNAs were significantly enriched (≥2-fold; adjusted $p < 0.05$) in MDA-MB-231^{MSC} when compared to control BCCs (Figure 1A): miR-199a-3p, miR-34a, miR-762, miR-214, miR-let-7b, and miR-1915. Semiquantitative real-time PCR (rtPCR-ΔΔct) was used to validate the microarray findings, and it confirmed a multifold induction of these miRNAs in MSC-activated BCCs (Figure 1B).

Among this set, miR-199a-3p particularly attracted our attention. Noticeably, miR-199a-3p levels exhibited the highest levels of enrichment in MDA-MB-231^{MSC} compared to the other MSC-triggered miRs, rising more than ~65-fold over those of controls (Figure 1B). Interestingly, miR-199a-3p upregulation, while not previously functionally correlated with human breast carcinoma development, has been observed in other cancer contexts, such as esophageal (Feber et al., 2011), gastric (Brenner et al., 2011), or lung (Sakurai et al., 2011) carcinomas, suggesting a potential role for miR-199a-3p in breast cancer pathogenesis.

We observed that the MDA-MB-231^{MSC} population continued to produce high levels of miR-199a-3p even after separation from MSCs (Figure S1A available online), suggesting that its induction was sustained and intrinsic to BCC^{MSC}. In this regard, miR-199a-3p derives from two separate genomic regions in humans: one located on chromosome 19 and the other on chromosome 1, comprising the miR-199a1 (A1) and miR-199a2 (A2) loci, respectively. We proceeded to determine the relative contributions of A1 or A2 to the levels of mature miR-199a-3p present in MDA-MB-231^{MSC} by assessing the levels of the distinct locus-specific miRNA precursor stem-loops (pri-miRs) using rtPCR-ΔΔct. These experiments revealed that both pri-miR-199a1 and pri-miR-199a2 were significantly increased in MDA-MB-231^{MSC}, with a slightly elevated contribution of A1 (~60%) compared to A2 (~40%) (Figure 1C). Interestingly, miR-199a2 is transcribed from an intronic sequence of the *DNM3OS* gene, which also encodes for miR-214. miR-214 was similarly identified in our profiling arrays as induced by ~15-fold in MDA-MB-231^{MSC} (Figure 1B) and likewise maintained elevated levels 3 days after separation from MSCs (Figure S1A). These observations suggest that miR-199a-3p (produced from the A1 and A2 loci) and miR-214 (produced form the A2 locus) are functionally coregulated in MDA-MB-231^{MSC}.

To probe whether the ability of MSCs to trigger miR-199a-3p and miR-214 upregulation in BCCs is idiosyncratic to the MDA-MB-231 model, we tested the response of other BCCs to MSCs. Indeed, admixture of MSCs to MCF7/Ras, T47D, and MDA-MB-435 cells caused significant upregulation of both miR-199a-3p and miR-214, albeit to different extents with differing ratios of miR-199a-3p/miR-214 (Figure 1D), likely a consequence of the relative contributions of A1 versus A2 loci in these systems.

Of note is that robust induction of miR-199a-3p and miR-214 by bone-marrow-derived MSCs required cell-cell contact between BCCs and MSCs (Figure S1B) and did not occur upon the contact of BCCs with phenotypically similar fibroblastic cells, such as WI-38 cells or panniculus-derived MSCs (ad-MSCs; Figure S1C). Interestingly, the contact of BCCs with human-breast-derived MSCs (Br-MSCs; derived from reduction mammoplasty) or activated fibroblasts (CAFs; derived from human breast tumors) resulted in only miR-199a-3p upregulation, and not that of miR-214 (Figure S1C). Together, these observations suggest that bone-marrow-derived MSCs may be uniquely capable of activating both A1 and A2 loci, while highlighting miR-199a-3p activation as a potential common element of the BCC response to activated stroma in multiple settings.

miR-199a and miR-214 Promote Metastasis and CSC Phenotypes

Because our miRNA profiling studies were conducted on whole BCC^{MSC} populations, we could not rule out the possibility that certain BCCs within the total population express both miR-199a-3p and miR-214 (i.e., where both loci, or the A2 locus alone, is active), while others express only miR-199a-3p (i.e., when A1 locus alone is active). Accordingly, we proceeded to model both possibilities, stably expressing exogenous miR-199a, or both miR-199a and miR-214, in MDA-MB-231 cells (BCC^{199a} and BCC$^{199a/214}$, respectively). The expression levels of the respective miRNAs in BCC^{199a} and BCC$^{199a/214}$, verified by rtPCR-ΔΔct and compared to control counterparts harboring an empty vector (BCC^{null}), showed >40-fold and >3-fold upregulation in miR-199a-3p and miR-214 levels, respectively (Figure S2A).

We first explored the malignant potential of BCC^{199a} and BCC$^{199a/214}$ by examining their tumorigenic and metastatic abilities compared to BCC^{null}. For this purpose, equal numbers of cells of each group were implanted subcutaneously into athymic Nude mice and allowed to form tumors for 10–14 weeks. While BCC^{199a} and BCC$^{199a/214}$ tumors did not differ from BCC^{null} tumors in average weight at the time of tissue harvest (~0.5–0.65 g; Figure 2A), enumeration of the GFP-positive BCC colonies in the lungs of the respective animals using fluorescence microscopy revealed that mice implanted with either BCC^{199a} or BCC$^{199a/214}$ had ~3-fold the average of lung metastases per gram of tumor when compared with BCC^{null} controls (Figures 2B and 2C). These experiments demonstrated an enhanced malignancy of BCC^{199a} and BCC$^{199a/214}$ in vivo and prompted us to further characterize their metastasis-associated phenotypic attributes in vitro.

In these regards, BCC^{199a} and BCC$^{199a/214}$ exhibited no proliferative advantage over their control counterparts in 2D culture conditions (Figure S2B). Furthermore, these cells did not display increased expression of mesenchymal markers, such as vimentin, N-cadherin, smooth muscle actin (SMA), or lysyl oxidase (LOX) at the mRNA and/or protein levels, and they exhibited some resurgence in E-cadherin mRNA expression (Figures S2C and S2D). In addition, BCC^{199a} and BCC$^{199a/214}$ manifested an ~50% reduced intrinsic motility compared to BCC^{null} in Boyden chamber motility assays (Figure S2E). These observations suggested that the increased metastasis observed in BCC^{199a} and BCC$^{199a/214}$ is manifested through pathways distinct from those governing proliferation, invasion, and motility.

Our group and others have previously demonstrated that MSC activation of BCCs increases the population of putative CSCs as demonstrated by multifold upregulation in ALDH1 positivity and mammosphere-forming capacities (El-Haibi et al., 2012; Liu et al., 2011). CSCs are characterized by their distinctive capacity for tumor initiation, a trait that is thought to be integral to metastatic colonization because disseminated cancer cells engender new growths at distant sites (Malanchi et al., 2012). Supporting

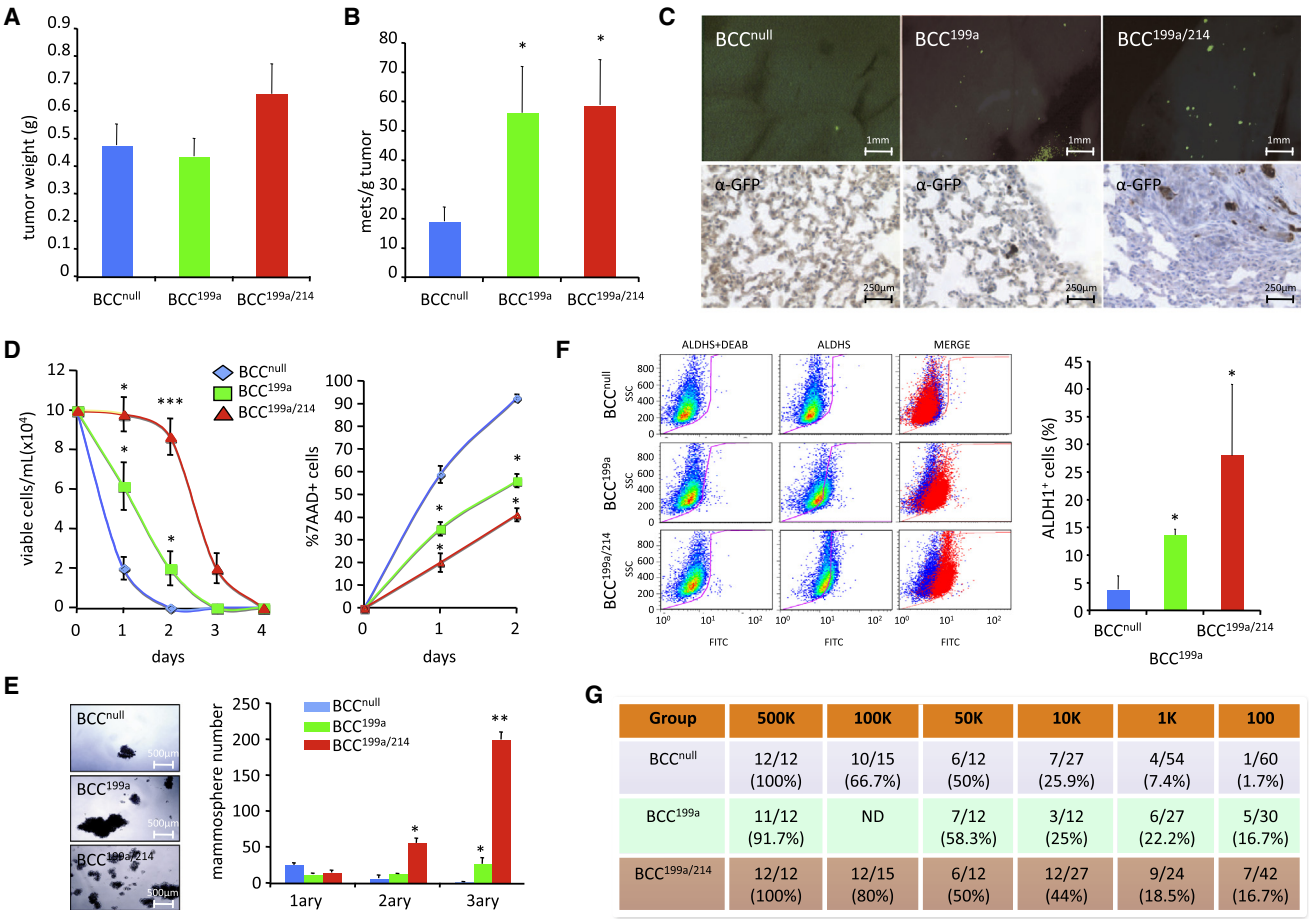

G

Group	500K	100K	50K	10K	1K	100
BCC^{null}	12/12 (100%)	10/15 (66.7%)	6/12 (50%)	7/27 (25.9%)	4/54 (7.4%)	1/60 (1.7%)
BCC^{199a}	11/12 (91.7%)	ND	7/12 (58.3%)	3/12 (25%)	6/27 (22.2%)	5/30 (16.7%)
$BCC^{199a/214}$	12/12 (100%)	12/15 (80%)	6/12 (50%)	12/27 (44%)	9/24 (18.5%)	7/42 (16.7%)

Figure 2. miR-199a and miR-214 Expression Causes Propagation of CSC Traits and Metastasis

(A) Mean weights (gram) ± SEM of matched tumors isolated from mice 8–14 weeks after implantation of BCC^{null} (n = 77), BCC^{199a} (n = 53), and $BCC^{199a/214}$ (n = 81).

(B) Metastatic index. Mean number of GFP-positive lung metastases ± SEM per gram of primary tumor burden per mouse. BCC^{null} (n = 37), BCC^{199a} (n = 27), and $BCC^{199a/214}$ (n = 37).

(C) Representative images of lung GFP-positive colonies in mice in (B). Upper panels: fluorescence microscopy; lower panels: anti-GFP immunohistochemistry.

(D) Minimal serum tumbling assay. Left: mean numbers of viable cells ± SEM, determined by trypan exclusion (n = 3). Right: percentage of apoptotic cells from left assessed by 7AAD staining/FACS analysis (n = 3).

(E) Sphere formation assay. Representative mean number of spheres in primary (1ary), secondary (2ary), and tertiary (3ary) passaged cultures ± SEM (n = 3).

(F) Left: representative ALDEFLUOR analyses of the indicated cells. DEAB, a specific inhibitor of ALDH1, was used as a control. Right: quantification of ALDEFLUOR assays (± SEM; n = 3).

(G) Tumor-initiation assay. Table indicating number of tumors initiated (>0.05 g) and total number of BCC injections per cell dilution (#cells/injection) is shown. p values calculated using ELDA (see Experimental Procedures) for BCC^{199a} and $BCC^{199a/214}$, respectively, are: 500K cell group: 0.232, 1; 100K cell group: 0.407; 50K cell group: 1,1; 10K cell group: 0.004, 0.152; 1K cell group: 0.064, 0.046; 100 cell group: 0.009, 0.005. *p < 0.05; **p < 0.01, ***p < 0.001 in two-tailed Student's t test.

See also Figure S2.

this notion, we observed that highly metastatic BCC^{MSC} exhibited increased tumorigenic properties in limiting dilution tumor-initiation analyses, forming subcutaneous tumors in Nude mice ~2.5 times more frequently than in controls, with as little as 100 cells per injection (Figure S2F).

With this information, we proceeded to determine whether the increased metastasis of BCC^{199a} and $BCC^{199a/214}$ correlated with their acquisition of CSC characteristics. Interestingly, BCC^{199a} and $BCC^{199a/214}$ displayed enhanced resistance to suspension-induced cell death in a minimal serum tumbling assay, exhibiting >50% survival rates after 24 hr of suspension, and a corresponding >50% reduction in their apoptosis rates as measured by 7-aminoactinomycin D (7AAD; Figure 2D). In addition, BCC^{199a} and $BCC^{199a/214}$ displayed increased abilities to grow in low-attachment mammosphere growth conditions after serial passages (Figure 2E), and they showed multifold increases in the expression levels of the CSC-associated marker ALDH1 (Ginestier et al., 2007), as determined by rtPCR (Figure S2G) and by ALDEFLUOR-based FACS assays (Figures 2F). Most importantly, however, BCC^{199a} and $BCC^{199a/214}$ possessed markedly enhanced tumor-initiating capabilities in limiting-dilution tumor assays in Nude mice, forming tumors at 100 cells per injection at ~2–3 times the rate of their BCC^{null} controls (Figure 2G). These observations suggested that the enhanced

metastasis of BCC^{199a} and BCC$^{199a/214}$ correlated with their acquisition of CSC-like traits.

We found that the enhanced metastasis-related phenotypes of BCC^{199a} were largely similar or identical to those of BCC$^{199a/214}$, suggesting that the promalignant activities of BCC$^{199a/214}$ rested largely on the actions of miR-199a. To distinguish between the effects of mature miR-199a-3p and miR-199a-5p, both of which are produced by stable expression of pre-miR-199a from our vector, we transfected individual RNA duplexes—offset to allow generation of only a specific single mature miRNA—coding for either *199a-3p* or *199a-5p* into MDA-MB-231 cells. While transient expression of *199a-3p* led to a significant ~2.5-fold increase in ALDH1 positivity, *199a-5p* expression did not (Figure S2H), despite substantial expression levels of *199a-5p* in these cells (Figure S2I). This suggested that miR-199a-3p is the critical miRNA produced from miR-199a in enhancing the observed population of putative CSCs.

In these regards, BCC^{199a} exhibited marked increases in the expression levels of additional breast CSC-associated markers, such as MYC (Figure S2J), GD2S, and POSTN (Figure S2K; (Liu et al., 2009; Malanchi et al., 2012; Battula et al., 2012; Nair et al., 2014). Furthermore, stable overexpression of miR-199a in other BCC lines, such as MCF7/Ras, T47D, or MDA-MB-435 cells, led to ~10-, ~6-, and ~4-fold increases, respectively, in their ALDH1 positivity (Figure S2L). Similarly, such expression caused upregulation of POSTN (Figure S2M) and the CD44^{high}/CD24^{low} population (Figure S2N) in T47D cells and increased MYC expression in MCF7/Ras cells (Figure S2J), suggesting that the ability of miR-199a-3p to regulate CSC phenotypes is not idiosyncratic of MDA-MB-231 cells. Notably, >65% of mice tail-vein-injected with BCC^{199a} exhibited lung metastases at limiting conditions where BCC^{null} controls exhibited none (Figure S2O), suggesting that the induction of CSC traits by miR-199a contributes to secondary tissue colonization.

Downregulation of the Speech Gene *FOXP2*, Observed in BCC^{199a} and BCC$^{199a/214}$, Promotes CSC Traits and Metastasis

We next aimed to elucidate the mechanistic details underlying the malignancy of BCC^{199a} and BCC$^{199a/214}$. For this purpose, we probed BCC^{199a} and BCC$^{199a/214}$ for the expression levels of >20 published targets for miR-199a-3p (or miR-214), but we did not find consistent downregulation of such targets in both BCC^{199a} and BCC$^{199a/214}$ as compared to BCC^{null} (Figures S3A and S3B; see Supplemental Information), underscoring the importance of cellular context in determining miRNA functions.

To identify potential miRNA effectors in BCC^{199a} and BCC$^{199a/214}$, we proceeded to utilize array-based approaches, focusing upon those that have been correlated with the acquisition or maintenance of stem-like properties. In these regards, we carried out a targeted rtPCR-ΔΔct array screen of 84 genes associated with stem cell maintenance or differentiation (QIAGEN), evaluating their relative mRNA levels in BCC^{199a} and BCC$^{199a/214}$ as compared to BCC^{null}. These analyses indeed identified a number of stem-cell-associated genes that were significantly upregulated in BCC^{199a} and/or BCC$^{199a/214}$, including GATA-binding protein-6/*GATA6* (Zhang et al., 2008), lin-28 homolog B/Lin28B (Zhou et al., 2013), homeobox C9/*HOXC9* (Okamoto et al., 2007), and msh homeobox 2/*MSX2* (Dorado et al., 2011). Surprisingly, only forkhead box P2/ *FOXP2* was found to be significantly (≥2-fold; $p < 0.005$) downregulated in both cell types, exhibiting 7- and 13-fold reductions in its expression levels in BCC^{199a} and BCC$^{199a/214}$, respectively (Figure S3B).

FOXP2 is a member of the forkhead family of transcription factors (Myatt and Lam, 2007). It has been described to act as a transcriptional repressor, primarily in the context of neural development and function (Spiteri et al., 2007). Its functions have been shown to be essential for developmental neurogenesis (Tsui et al., 2013), for neuronal plasticity, and for the capacity for human speech (Fisher and Scharff, 2009). FOXP2 has likewise been shown to serve an essential role in the development and differentiation of nonneuronal tissues, such as lung and esophagus (Shu et al., 2007; Shu et al., 2001). However, a causal role for FOXP2 deregulation in breast cancer pathogenesis has not been established. We validated the array results regarding *FOXP2* using independent rtPCR-ΔΔct analyses (Figure 3A), and we further found that its protein levels were severely repressed in both BCC^{199a} and BCC$^{199a/214}$ (Figure 3B), as well as in BCC^{MSC} (Figure 3C). Because loss of FOXP2 was shown to preserve progenitor cell identity and block differentiation in the abovementioned contexts, we hypothesized that FOXP2 downregulation might play a role in defining the CSC-like phenotypes of BCC^{199a}, BCC$^{199a/214}$, and BCC^{MSC}.

We tested this possibility first by probing for *FOXP2* levels in the FACS-enriched ALDH1-positive fractions of MDA-MB-231^{MSC}. Indeed, ALDH1-positive cells, which possess tumor-initiating capacities (forming 60% tumors at 10,000 cells per injection compared to ALDH1-negative counterparts; Figure S3C), exhibited a striking >95% reduction in their *FOXP2* content (Figure 3D). Furthermore, expression of miR-199a in T47D cells, which enhanced their CSC-like characteristics (Figures S2L-S2N), also prompted a marked downregulation of FOXP2 (Figure 3E). These findings correlated FOXP2 downregulation with the propagation of CSC-like traits.

To determine the functional consequences of FOXP2 inhibition on the induction of CSC-like phenotypes and breast cancer progression, eight different retroviral plasmids expressing various short-hairpin RNAs designed for knockdown of *FOXP2* (shFOXP2) were stably expressed in MDA-MB-231 cells (BCC^{shFOXP2}). The functionality of each hairpin was verified by western blot analyses, and this revealed two efficient hairpins, shFOXP2-1.5 and shFOXP2-2.2, that precipitated an ~70% reduction of FOXP2 protein levels (Figure 4A). When probed with ALDEFLUOR, BCC$^{shFOXP2\text{-}1.5}$ and BCC$^{shFOXP2\text{-}2.2}$ exhibited significant (>40- and >10-fold, respectively) upregulation in their ALDH1 positivity compared to control cells expressing a scrambled hairpin control (BCC^{shSCRAM}; Figures 4B and S4A). In addition to increases in their ALDH1 positivity, shFOXP2-expressing cells also exhibited increases in *OCT4* (Figure S4B) and c-Myc (Figures 4C and S4C) and a 2-fold increase in their CD44^{high}/CD24^{low} populations (Figure S4D). Furthermore, shFOXP2 expression enhanced mammosphere colony formation in suspension by an average of ~2.5-fold (Figure 4D) and provided BCCs with enhanced abilities to resist anoikis (Figure S4E). Most importantly, BCC$^{shFOXP2\text{-}2.2}$ initiated subcutaneous tumors in Nude mice at a frequency of 28% and with as little as 100 cells per injection, a dilution prohibitive for BCC^{shSCRAM} (Figure 4E).

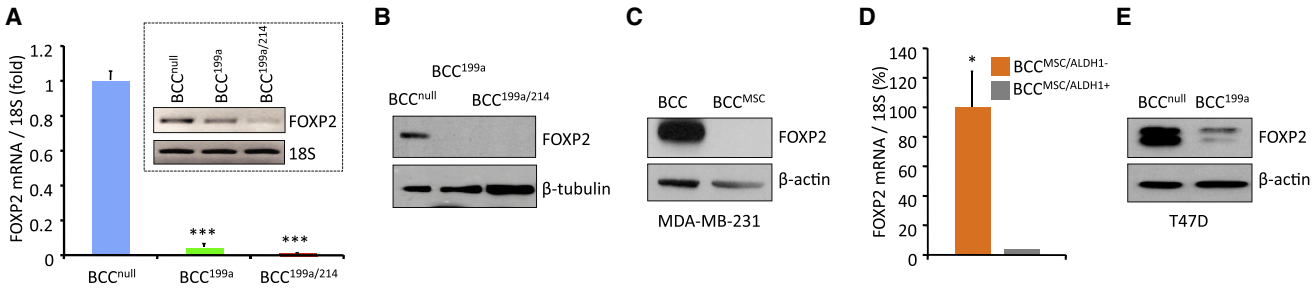

Figure 3. A Targeted PCR Screen Identified FOXP2 as a Putative Target in BCC^{199a} and BCC$^{199a/214}$

(A) Representative rtPCR-ΔΔct probing *FOXP2* in the indicated cell lines (± SEM; n = 3). Inset: DNA gel from rtPCR-ΔΔct.

(B) Western blot probing for FOXP2 in whole lysates as indicated. β-tubulin was used as a loading control (n = 3).

(C) Western blot for FOXP2 in whole-cell lysates of resting or MDA-MB-231^{MSC} cells. β-actin was used as a loading control (n = 3).

(D) rtPCR-ΔΔct analysis showing relative abundance of *FOXP2* mRNA in FACS-fractionated ALDH1-positive versus ALDH1-negative MDA-MB-231^{MSC} cells (± SEM; n = 3).

(E) FOXP2 western blot in the indicated whole T47D lysates (n = 2). β-actin was used as a loading control.

*p < 0.05; ***p < 0.001 in two-tailed Student's t test. See also Figure S3.

These results indicated that FOXP2 inhibition produces cells with in vitro and in vivo phenotypes consistent with those of CSCs.

Mirroring the phenotypes of BCC$^{199a/214}$, BCC^{shFOXP2} did not exhibit enhanced proliferation in vitro (Figure S4F) or enhanced tumor growth in vivo (Figure 4F). However, mice bearing BCC^{shFOXP2} tumors exhibited a dramatic ~9-fold increase in the numbers of metastatic lung foci per gram of primary tumor as compared to controls bearing BCC^{shSCRAM} tumors (Figures 4G and 4H). Altogether, these results demonstrate that FOXP2 inhibition is sufficient to promote the propagation of CSC-like phenotypes in BCCs, paralleling an observed marked enhancement of metastasis.

FOXP2 Downregulation and miR-199a-3p Upregulation Are Prominent Features of Aggressive Clinical Breast Cancer

We sought to determine the clinical relevance of our findings, first concentrating on whether *FOXP2* downregulation represents a feature of clinical breast cancer. For this purpose, we mined the recently published breast cancer sequencing data made available by the Cancer Genome Atlas Network (2012), and we found *FOXP2* to be downregulated ~4-fold in primary breast tumors as compared to normal tissues (Figure S5A). Importantly, we found that *FOXP2* levels were repressed ~2-fold in invasive ductal breast carcinomas (IDCs) as compared to benign lesions (Figure S5B; Chen et al., 2010). To explore whether *FOXP2* depression is associated with particular breast cancer subtypes, we interrogated publicly available luminal A, luminal B, HER2-enriched, and basal-like breast tumor expression data sets (Pawitan et al., 2005; Dedeurwaerder et al., 2011; Sabatier et al., 2011). These analyses revealed *FOXP2* downregulation as a common feature of all these subtypes (Figures 5A, S5C, and S5D) and were mirrored by our own rtPCR-ΔΔct analysis on RNA derived from macrodissected breast cancers, in which we observed a striking ~80% *FOXP2* repression across tumor samples (n = 74) when compared to RNA derived from normal tissues (n = 5; Figure 5B). Importantly, we found that low FOXP2 expression inversely correlated with overall disease-free survival (Figure 5C), as well as distant metastasis-free survival (Figure 5D) in independent cohorts, suggesting that *FOXP2* repression is indicative of increased malignancy in clinical breast cancer.

Similarly, we found miR-199a-3p levels to be elevated in IDC samples compared to in situ ductal cancers (Figure S5E; Farazi et al., 2011; Volinia et al., 2012). Within IDC, miR-199a-3p levels correlated with disease progression and associated significantly with lymph node positivity (N1 or N2) in a study of >600 breast cancer patients (Figure 5E; Cancer Genome Atlas Network, 2012). Most interestingly, miR-199a-3p levels were significantly elevated in primary tumors of patients who exhibited relapse (Figure 5F) and also correlated with decreased patient survival over 5- and 10-year intervals (Figures 5G). Collectively, these observations suggested that deregulation of FOXP2 and miR-199a-3p are common features of breast cancer progression and highlight important prognostic values for these players in breast cancer pathogenesis.

FOXP2 Is a Common Target for a Converging and Interrelated Set of MSC-Regulated miRNAs

We aimed to gain molecular insight into the regulation of *FOXP2* by MSC-induced miR-199a-3p. We analyzed the proximal (~1 kb) *FOXP2* 3′ UTR for consensus miRNA seed sites using in silico miRNA target prediction algorithms, such as RNAhybrid, miRWalk, Targetscan, and Pictar, but we were unable to find strong consensus seed sites for miR-199a-3p with the predicted free energy cutoff of ≤ -25 kcal/mol. However, these approaches did reveal putative target sites for each of the other miRNAs induced in BCC^{MSC}, namely miR-762, miR-let-7b, miR-34a, and miR-1915 (Figures S6A and S6B). For this reason, we tested the capability of these particular miRNAs in repressing *FOXP2* mRNA expression. Indeed, stable expression of miR-762 or miR-1915, or transient expression of miRNA mimics for miR-let-7b or miR-34a (Figure S6C), brought about a significant reduction in FOXP2 levels in MDA-MB-231 cells (Figures 6A and 6B). Consistent with FOXP2 downregulation, these cells exhibited an increase in ALDH1 positivity as determined by ALDEFLUOR assays, displaying ~20-, ~75-, ~30-, and ~30-fold increases by miR-let-7b, miR-34a, miR-762, and miR-1915, respectively (Figure 6C).

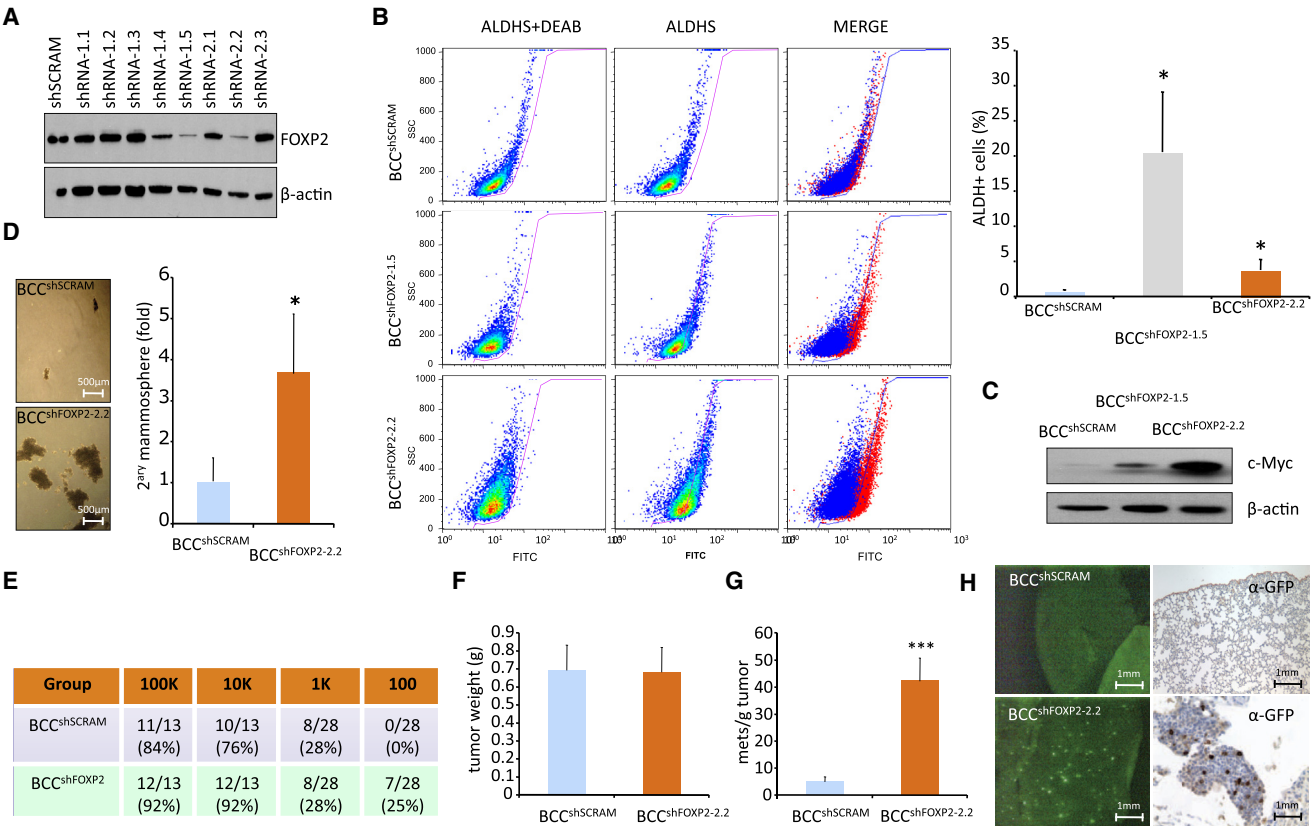

Group	100K	10K	1K	100
BCC^{shSCRAM}	11/13 (84%)	10/13 (76%)	8/28 (28%)	0/28 (0%)
BCC^{shFOXP2}	12/13 (92%)	12/13 (92%)	8/28 (28%)	7/28 (25%)

Figure 4. FOXP2 Downregulation Drives CSC Phenotypes and Metastasis

(A) FOXP2 western blot after knockdown by the indicated shRNAs.

(B) Representative ALDEFLUOR analyses of the indicated cell lines (n = 4). DEAB was used as a control.

(C) Representative western blot for c-Myc in whole-cell lysates of the indicated MDA-MB-231 cells. β-actin was used as a loading control (n = 3).

(D) Sphere formation assay. Representative images and quantification of secondary spheres (n = 3).

(E) Tumor-initiation assay. Table indicates the number of tumors initiated (>0.05 g) and the total number of BCC injections for each cell dilution (#cells/injection). Respective p values for BCC^{shSCRAM} and BCC^{shFOXP2} calculated by ELDA were as follows: 100K cells group: 0.536; 10K cells group: 1; 1K cells group: 0.736; 100 cells group: 0.0375.

(F) Mean weight (grams) ± SEM of matched subcutaneous primary tumors derived from Nude mice after 8–14 weeks of BCC^{shSCRAM} (n = 30) or BCC^{shFOXP2} (n = 46) injections.

(G) Metastatic index. Mean numbers of GFP-positive lung metastases ± SEM per gram of primary tumor burden per mouse are shown; n = 16 for BCC^{shSCRAM} and n = 25 for BCC$^{shFOXP2\text{-}2.2}$.

(H) Representative images of GFP-positive colonies and anti-GFP IHC in the lungs of BCC^{shSCRAM} or BCC$^{shFOXP2\text{-}2.2}$ mice in (G).

*p < 0.05; ***p < 0.001 in two-tailed Student's t test. See also Figure S4.

Based on these results and the fact that miR-199a-3p was not predicted to target the proximal 3′ UTR of *FOXP2*, we asked if miR-199a might repress *FOXP2* through the actions of these four miRNAs. Indeed, we found that the expression levels of miR-let-7b, miR-34a, miR-762, and miR-1915 were all elevated ~7-, ~4.5-, ~5-, and ~4.5-fold, respectively, in BCC$^{199a/214}$ (Figure 6D), suggesting a coregulatory relationship gathering these miRs with miR-199a-3p. In support of this notion, and using targeted qPCR assays, we found that the expression levels of miR-199a-3p in clinical breast cancer specimens correlated with the expression levels of miR-let-7b, miR-34a, and miR-1915 (Figure 6E; we were unable to test miR-762 because the sensitivity of the assay necessitated the use of prohibitively large amounts of primary RNA material). These findings are consistent with the existence of an operational crosstalk between MSC-induced miRNAs in BCCs and highlight one mechanism through which miR-199a-3p represses FOXP2 expression. Of translational importance, high concerted expression levels of miR-199a-3p, miR-let-7b, miR-34a, and miR-1915 were indicative of overall poorer survival in breast cancer patients as assessed by Kaplan-Meier analyses (Figure 6F) and Cox multivariate analysis (Figure S6D), suggesting that the described miR network represents a powerful and significant prognostic indicator in clinical breast cancer. These results reveal functional cooperation between members of an interrelated regulatory network of miRNAs, led by miR-199a, which converge to inhibit the expression of *FOXP2* and thereby promote tumor initiation and metastasis (Figure 6G).

DISCUSSION

By probing for BCC miRNAs deregulated by MSC stimulation, we identified a set of interrelated miRs whose actions converge

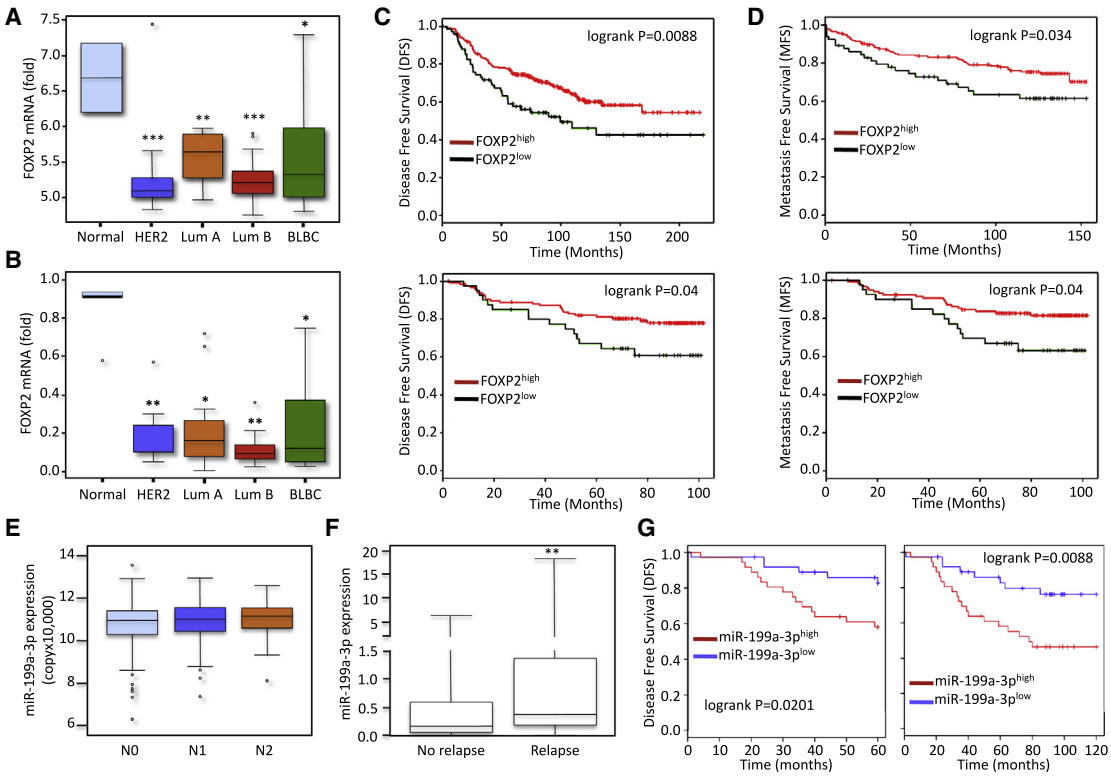

Figure 5. Upregulation of miR-199a and Downregulation of FOXP2 in Clinical Breast Cancer

(A) *FOXP2* levels (Log2) in normal versus the indicated breast cancer subtypes in GSE20711. p values for normal (n = 2) versus HER2 (n = 26), Lum A (n = 13), Lum B (n = 22), and BLBC (n = 27) were 0.0005325, 0.001527, $4.573 \times e^{-6}$, and 0.03824, respectively. Significance was determined using unpaired Student's t test.

(B) *FOXP2* rtPCR-ΔΔct on macrodissected breast cancer specimens derived from HER2 (n = 12), Lum A (n = 25), Lum B (n = 25), and BLBC (n = 12) subgroups versus normal (n = 5). Significance was determined using unpaired Student's t test.

(C) Upper: disease-free survival of high- and low-*FOXP2* expression groups from van de Vijver (2002) NKI platform (n = 221 and 74, respectively). Reporter Contig used was 35884_RC, HR = 1.7(1.1 − 2.6), and Chi-square p = 0.016. Lower: disease-free survival analyses performed on high- and low-*FOXP2* expression groups in Pawitan et al. (2005) platform HG-U133B (n = 119 and 40, respectively). Reporter used was 243278_at, HR = 1.9(1.0 − 3.7), and Chi-square p = 0.041.

(D) Upper: metastasis-free survival analyses from Miller (2005) using platform HG_U133B (n = 195 and 65, respectively). Reporter used was 235201_at, HR = 1.7(1.0 − 2.8), and Chi-square p = 0.046. Lower: disease-free survival analyses performed on high- and low-*FOXP2* expression groups in Pawitan et al. (2005), platform HG-U133B (n = 119 and 40, respectively). Reporter used was 243278_at, HR = 2.2(1.1 − 4.2), and Chi-square p = 0.025.

(E) miR-199a-3p expression in IDC patients (n = 664; Cancer Genome Atlas Network, 2012) with or without lymph node positivity. N0 geometric mean RPM is 1780.7 (n = 301), N1 geometric mean is 1951.8 (n = 223), and N2 geometric mean is 2141.3 (n = 82). Spearman correlation test N0 < N1 < N2, p = 0.013.

(F) Normalized miR-199a-3p levels (rtPCR-ΔΔct) on primary-tumor-derived RNA in relapse-free breast cancer patients (n = 34) versus relapsed patients (n = 40) in Cimino et al. (2013). Mann-Whitney p = 0.029 and Wilcoxon p = 0.0193.

(G) miRNA-199a-3p median fold change (FC) stratified the independent populations in Cimino et al. (2013) into two groups, which were significantly different in their survival probability (n = 73).

See also Figure S5.

to downregulate the developmental transcription factor FOXP2. We demonstrated that expression of these miRs or knockdown of FOXP2 was sufficient to increase breast CSC-like traits, fostering increased tumor-initiating abilities and enhancing tumor metastasis. These results incriminate miRNA-regulated pathways in breast CSC propagation and metastasis and describe an involvement of the speech-associated transcription factor FOXP2 in regulating breast cancer malignancy, thereby providing mechanistic insights into breast cancer pathogenesis.

A series of studies have described the enrichment of A1 and A2 loci miRNAs in cancer tissues. Indeed, miR-199a expression has been found to be elevated in a number of solid malignancies, such as lung cancer (Mascaux et al., 2009), colorectal cancer (Wan et al., 2013), ovarian cancer (Iorio et al., 2007), and melanoma (Pencheva et al., 2012). Similarly, upregulated levels of miR-214 have been reported in ovarian (Yang et al., 2008), pancreatic (Zhang et al., 2010), and oral (Scapoli et al., 2010) cancers. In breast, two reports have described increased levels of miR-199a-3p in malignant myoepithelioma of the breast (Bockmeyer et al., 2011) and elevated miR-214 levels in the blood of patients diagnosed with malignant breast tumors (Schwarzenbach et al., 2012). Despite these intriguing studies, the functional contributions of miR-199a and miR-214 to breast cancer progression were unknown. Recently, miR-199a has been shown to target apolipoprotein E (ApoE) and the heatshock factor DNAJA4 in the context of melanoma, which was shown to relieve the inhibitory influence of ApoE on endothelial

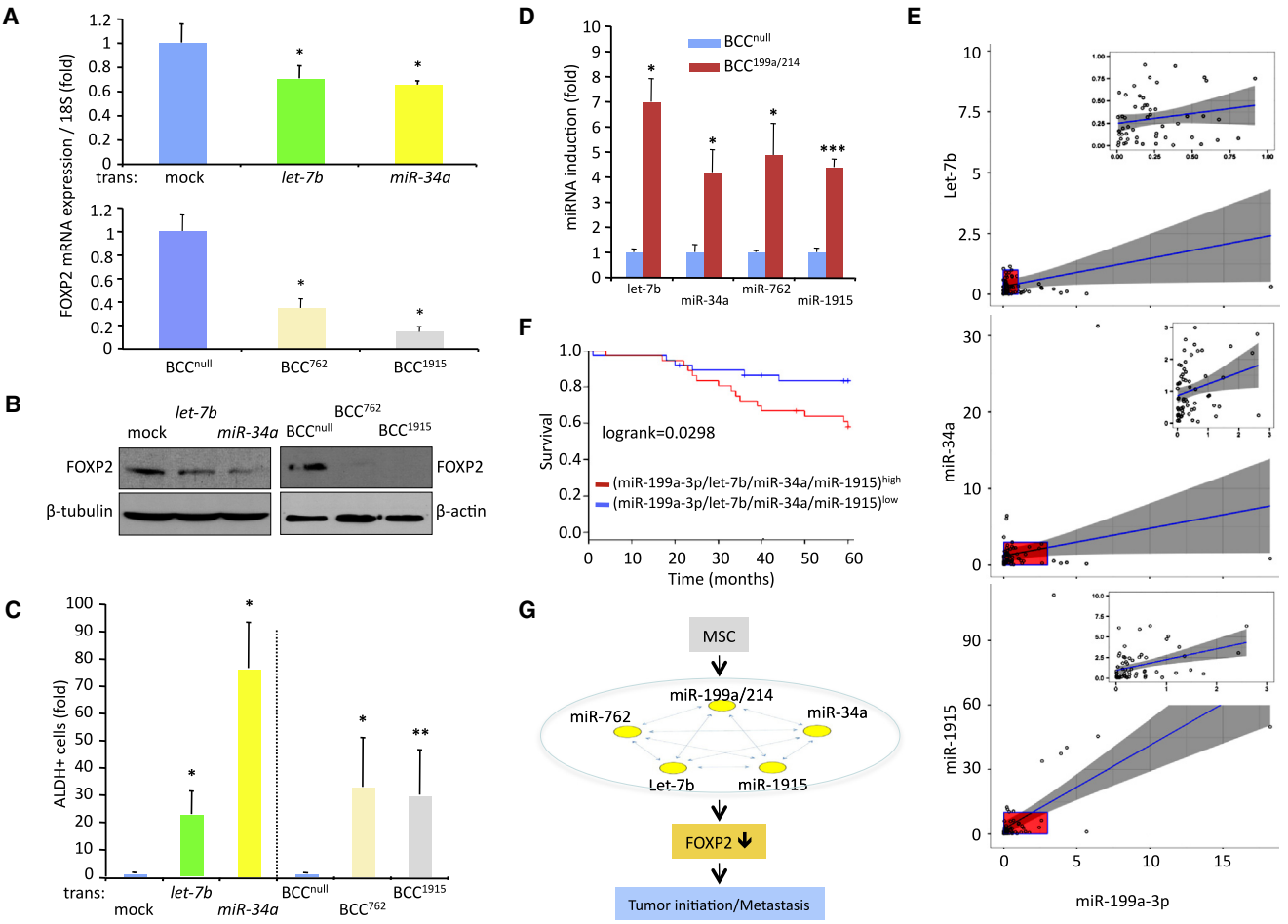

Figure 6. MSC-Induced miRNAs Converge on FOXP2

(A) Upper: rtPCR-ΔΔct for FOXP2 mRNA levels in MDA-MB-231 cells transiently transfected with miR-let-7b or miR-34a mimics compared to mock. (± SEM; n = 3). Lower: rtPCR-ΔΔct of *FOXP2* in MDA-MB-231 cells stably expressing miR-762 (BCC^{762}), miR-1915 (BCC^{1915}), or controls (BCC^{null}) (± SEM; n = 3).

(B) Western blots showing FOXP2 levels in MDA-MB-231 whole lysates of BCC^{null}, BCC^{762}, or BCC^{1915} (left) or in BCCs transiently transfected with miR-let-7b or miR-34a mimics (right) (n = 3).

(C) Relative fold ALDH1-positive cells compared to controls in the indicated groups in (B) (± SEM; n = 3).

(D) rtPCR-ΔΔct for the indicated miR in BCC^{null} and $BCC^{199a/214}$ (± SEM; n = 3).

(E) Pearson coefficient of miRNA fold changes shows significant correlations between expression levels of miR-199a-3p and miR-1915, miR-let-7b, and miR-34a, as determined by rtPCR-ΔΔct on clinical samples from Cimino et al. (2013).

(F) Median fold change (FC) of the combined expression levels of miR-199a-3p, miR-34a, miR-let-7b, and miR-1915 stratify the population in Cimino et al. (2013) into two groups with different 5 year survival probability (n = 73).

(G) Model: MSC stimulation of BCCs induces a set of miRNAs, led my miR-199a/214, which converge on FOXP2. The downregulation of FOXP2 is sufficient to promote tumor initiation and metastasis.

*p < 0.05; **p < 0.01, ***p < 0.001 in two-tailed Student's t test. See also Figure S6.

recruitment, thereby affording cancer colonies with enhanced vascularization (Pencheva et al., 2012). While we cannot rule out similar paracrine actions of miR-199a/214 in our models, we did not find *ApoE* and *DNAJA4* to be downregulated in MDA-MB-231 stably expressing these miRNAs, underscoring the importance of cell context in miRNA targeting of complementary mRNAs. Here, we have elucidated an ostensibly autocrine mechanism of action for A1 and A2 loci miRNAs in breast carcinoma pathogenesis.

To determine how BCC^{199a} and $BCC^{199a/214}$ acquire their malignant phenotypes, we tested the expression levels of a large subset of published targets for miR-199a, but we were unable to verify consistent target downregulation across BCC^{199a}, $BCC^{199a/214}$, and BCC^{MSC}. Influenced by the observations that BCC^{199a}, $BCC^{199a/214}$, and BCC^{MSC} acquired CSC-like traits, we conducted stem-cell-factor-focused screens and identified FOXP2 as a factor that was significantly and consistently repressed in all three conditions.

FOXP2 is a transcription factor that has been tightly linked to nervous system development, encompassing activities that range from neuronal maturation to axonal guidance and speech regulation (Fisher and Scharff, 2009; Tsui et al., 2013; Vernes et al., 2011). On the molecular level, FOXP2 functions in transcriptional repressor complexes, which downregulate the

expression of a multitude of targets involved in lineage determination (Shu et al., 2001; Li et al., 2004; Shu et al., 2007; Konopka et al., 2009). However, to our knowledge, functions for FOXP2 in breast cancer development have not been previously reported. We found FOXP2 downregulation to be sufficient for enhanced tumor-initiating and metastatic abilities of cancer cells in animals, and we further observed *FOXP2* to be significantly downregulated across multiple clinical subtypes of breast cancers. Particularly, we observed that HER2-enriched tumors exhibited a reproducible and statistically significant 4-fold downregulation of *FOXP2* (and ~2.5-fold increase in miR-199a-3p) when compared to the BLBC subtype (Figure S5F), suggestive of a preferential enrichment for this pathway in HER2 breast cancer. Interestingly, HER2 tumors displayed increased SMA-positive fibroblastic cell infiltrates (consistent with CAF/MSC-like cells) when compared to BLBC (Toullec et al., 2010; data not shown), which draws a strong association between CAF/MSC tumor content and a depression of *FOXP2* expression in clinical breast cancer. Furthermore, we found that expression of a UTR-free *FOXP2* cDNA in BCCs in the context of miR-199a overexpression or in the background of MSC stimulation significantly inhibited both lung colonization (Figure S4G) and ALDH1 positivity (Figure S4H). Together, these observations strongly suggest that FOXP2 plays a critical role in breast cancer pathogenesis. It remains unclear as to whether FOXP2 exerts these activities via transcriptional repression and whether its downregulation in clinical breast cancer is an event that occurs early or late in tumor development. Because of its involvement in tumor initiation and metastasis, we hypothesize that FOXP2 may serve dual roles, both in tumorigenesis and in tumor progression to metastasis. Efforts to decipher the molecular mode of action of FOXP2 in breast cancer initiation, maintenance, and progression are currently underway.

The present work also highlights pathways utilized by tumor-associated MSCs to foster the malignancy of BCCs. Previous work from our group and others has shown that the contact between MSCs and BCCs resulted in gene expression changes in both cell types, favoring the development of a microenvironment that is conducive to metastatic progression. Indeed, BCC-activated MSCs primarily produce the chemokine CCL5, which acts back on the neighboring BCCs in a paracrine fashion and through CCR5, fostering their invasive migration and increased lung colonization (Karnoub et al., 2007; Chaturvedi et al., 2013). Similarly, we previously reported that MSC-activated BCCs are most enriched in EMT markers and phenotypes, mechanisms predominantly mediated by LOX via a CD44-Twist signaling axis (El-Haibi et al., 2012). Importantly, we observed that neither CCL5 (Figures S1D and S1E) nor LOX (Figure S1F) was sufficient in triggering CSC-associated miR-199a-3p/miR-214 expression, consistent with our previous results that CCL5 and LOX do not foster CSC-like traits in cancer cells (data not shown; El-Haibi et al., 2012). Intriguingly, and despite these observations, we found that TWIST1 expression in the cancer cells was sufficient to promote miR-199a-3p and miR-214 expression (Figure S1G) as well as FOXP2 repression (Figure S1H) and that it was critically required for the induction of the A1/A2 loci by MSCs (Figure S1I). These results are indicative of a complex crosstalk operating between MSC-driven EMT and CSC machineries and are suggestive of independent outside-in signaling axes regulating miR-199a in multiple BCC^{MSC} (e.g., Figure S1J).

Metastatic progression requires cancer cells to overcome dissimilar obstacles related to loss of adhesion and local invasion, intra/extravasation, and reacquisition of adhesion and proliferative capacities for colonization of inhospitable secondary tissues. It is plausible to reason that negotiating these sequential steps would require reversible shifts in gene expression programs. For this reason, studying the steady state stable transcriptional profiles of metastatic nodules may not provide a comprehensive understanding of the otherwise obligatorily plastic pathways that contribute to the establishment of secondary cancer colonies. In these regards, the MSC-induced model of tumor metastasis, which has gained increased attention over the past few years, possesses distinct advantages that enable the discovery of temporal, stroma-instigated pathways that permit cancer cells to execute the multiple steps of the metastasis cascade.

EXPERIMENTAL PROCEDURES

Detailed procedures can be found in the Supplemental Information.

Cells

BCCs were cultured using standard protocols described elsewhere (Karnoub et al., 2007; El-Haibi et al., 2012). Primary BCCs DT22 and DT28 are described elsewhere (Drews-Elger et al., 2014). Primary human bone marrow MSCs (BM-MSCs), primary ad-MSCs, Br-MSCs, and WI-38 human embryonic lung fibroblasts were propagated as previously described (El-Haibi et al., 2012; Hanson et al., 2013) and utilized before passage 5. CAFs were described previously (Hu et al., 2008).

Cocultures and Sorting

For direct cocultures, MSCs, CAFs, or WI-38 cells were cocultured with GFP-BCCs (at 3:1 ratio) for 72 hr (e.g., El-Haibi et al., 2012). All cells were cultured individually in parallel as controls. GFP-BCCs were recovered by FACS and processed as described below. For indirect cocultures, MSCs and BCCs were grown for 72 hr across 0.4 μm membrane in a Boyden chamber setup, and BCCs were collected and processed for RT-qPCR determinations as described below.

Agilent Arrays

An Agilent oligonucleotide microarray system (miRNA AMADID 025987, Agilent Technologies) was used to detect miRNA gene variation in MDA-MB-231 stimulated with BM-MSCs as compared to controls.

rtPCR-ΔΔct Analysis and Primers

Total RNA was extracted using miRNeasy kit (QIAGEN) and was processed for reverse transcriptase with a miScript II RT kit and via qPCR using standard procotols. Miscript primers used and primer sequences are listed in the Supplemental Information.

Constructs

pRRL3-GFP-BCCs were previously described (El-Haibi et al., 2012). For stable miRNA overexpression, GFP-BCCs were transfected with pEGP-miR Null, pEGP-miR-199a-2 (Cell Biolabs), or pcDNA3.2/V5 hsa-mir-214 (D. Bartel) and stable transfectants were selected with puromycin and/or G418. pEGP-miR-1915 and pEGP-miR-762 were generated by PCR amplification of precursor stem-loops from human genomic DNA and were subcloned into a miRNA Select pEGP-miR (Cell Biolabs). QIAGEN miScript miRNA Mimics #MSY0000232 and # MSY0000231 were used for expression of miR-199a-3p and miR-199a-5p. #MSY0000063 and #MSY0000255 RNA duplexes (QIAGEN) were used for expression of miR-let-7b-5p and miR-34a-5p, respectively. pLKO.1 FOXP2 shRNAs and shSCRAM constructs (Dana-Farber Cancer Institute) were stably expressed in MDA-MB-231 as standard. The long-form (variant 2) of FOXP2 was purchased from Origene.

Proliferation Assays, Western Blotting, Transwell Motility, Anoikis, ALDEFLUOR, and Sphere Formation Assays

These assays were conducted using standard procedures described in detail in the Supplemental Information.

Tumor Initiation and Metastasis Analyses

Female athymic Nude mice (Charles River Laboratories #490) were subjected to 200 μl (2:1 complete DMEM/cells:Reduced Growth Factor Matrigel; BD Biosciences) subcutaneous injections of BCCs. Tumorigenesis was assessed via palpation and confirmed by fluorescence microscopy after excision. Statistical analyses were performed utilizing ELDA: Extreme Limiting Dilution Analysis software (Hu and Smyth, 2009). Fluorescence microscopy was used to assess lung metastasis.

PCR Profiling Arrays

BCC-derived RNA was analyzed using Human Stem Cell PCR Array (QIAGEN #PAHS-501Z), and data was analyzed using RT^2 Profiler PCR Array Data Analysis software (http://www.sabiosciences.com/pcrarraydataanalysis.php).

Clinical Analyses

FOXP2 determinations were derived from ROCK (Cancer Genome Atlas Network, 2012; Chen et al., 2010); from GSE20711, GSE21653, and GSE1456; or from tumors collected under approved Curie IRB protocols. miRNA determinations were derived from Farazi et al. (2011), from Cancer Genome Atlas Network (2012), from breast cancer samples in Cimino et al. (2013), or from the Curie set.

SUPPLEMENTAL INFORMATION

Supplemental Information for this article includes six figures and Supplemental Experimental Procedures and can be found with this article online at http://dx.doi.org/10.1016/j.stem.2014.10.001.

AUTHOR CONTRIBUTIONS

B.G.C. and A.E.K. designed research; and B.G.C., A.C., G.W.B., A.L., F.O., E.C.L., M.K.B., M.R., F.M.G., S.V., A.V.S., D.T., and A.E.K. performed research and collected and analyzed data. S.E.H., A.M., D.E.A., P.H., and K.P. provided primary cells; O.M. provided clinical specimens; B.G.C. and A.E.K. wrote and edited the paper; and A.E.K. directed and supervised research.

ACKNOWLEDGMENTS

We thank J. Love, J.-A. Kwon, and S. Gupta for miRNA profiling data analysis; A. Contreras for assistance in animal studies; K. Groglio and M. Fahlberg for FACS sorting assistance; D. Louvard for assistance in clinical specimen procurement; and P. Pandolfi and P. Provero for helpful discussions. This work was supported by start-up funds from BIDMC (A.E.K.), the Sidney Kimmel Cancer Research Foundation (A.E.K.), the Susan G. Komen For The Cure (A.E.K.), AIRC IG14201 (D.T.), Compagnia di San Paolo, 2008.1054 (D.T.), and Progetto Ricerca Ateneo Torino (D.T.). Human BM-MSCs were provided by the Texas A&M Health Science Center (CMI for Regenerative Medicine at Scott & White) through NIH P40RR017447. B.G.C. is a 2012 American Cancer Society Postdoctoral Fellow. F.O. is a recipient of FIRB giovani 2008 (RBFR08F2FS-276 002). A.E.K. is a 2010 Kimmel Scholar, a recipient of a Career Development Award from the BIDMC Prostate and Breast Cancer Research Program, and a recipient of a 2012 Career Catalyst Research Award from Susan G. Komen For The Cure.

Received: November 6, 2013
Revised: June 27, 2014
Accepted: October 2, 2014
Published: October 16, 2014

REFERENCES

Barcellos-Hoff, M.H., Lyden, D., and Wang, T.C. (2013). The evolution of the cancer niche during multistage carcinogenesis. Nat. Rev. Cancer *13*, 511–518.

Bartel, D.P. (2009). MicroRNAs: target recognition and regulatory functions. Cell *136*, 215–233.

Battula, V.L., Shi, Y., Evans, K.W., Wang, R.Y., Spaeth, E.L., Jacamo, R.O., Guerra, R., Sahin, A.A., Marini, F.C., Hortobagyi, G., et al. (2012). Ganglioside GD2 identifies breast cancer stem cells and promotes tumorigenesis. J. Clin. Invest. *122*, 2066–2078.

Bockmeyer, C.L., Christgen, M., Müller, M., Fischer, S., Ahrens, P., Länger, F., Kreipe, H., and Lehmann, U. (2011). MicroRNA profiles of healthy basal and luminal mammary epithelial cells are distinct and reflected in different breast cancer subtypes. Breast Cancer Res. Treat. *130*, 735–745.

Brenner, B., Hoshen, M.B., Purim, O., David, M.B., Ashkenazi, K., Marshak, G., Kundel, Y., Brenner, R., Morgenstern, S., Halpern, M., et al. (2011). MicroRNAs as a potential prognostic factor in gastric cancer. World J. Gastroenterol. *17*, 3976–3985.

Cancer Genome Atlas Network (2012). Comprehensive molecular portraits of human breast tumours. Nature *490*, 61–70.

Chaturvedi, P., Gilkes, D.M., Wong, C.C., Kshitiz, Luo, W., Zhang, H., Wei, H., Takano, N., Schito, L., Levchenko, A., and Semenza, G.L. (2013). Hypoxia-inducible factor-dependent breast cancer-mesenchymal stem cell bidirectional signaling promotes metastasis. J. Clin. Invest. *123*, 189–205.

Chen, D.T., Nasir, A., Culhane, A., Venkataramu, C., Fulp, W., Rubio, R., Wang, T., Agrawal, D., McCarthy, S.M., Gruidl, M., et al. (2010). Proliferative genes dominate malignancy-risk gene signature in histologically-normal breast tissue. Breast Cancer Res. Treat. *119*, 335–346.

Cimino, D., De Pitta, C., Orso, F., Zampini, M., Casara, S., Penna, E., Quaglino, E., Forni, M., Damasco, C., Pinatel, E., et al. (2013). miR148b is a major coordinator of breast cancer progression in a relapse-associated microRNA signature by targeting ITGA5, ROCK1, PIK3CA, NRAS, and CSF1. FASEB J *27*, 1223–1235.

Cuiffo, B.G., and Karnoub, A.E. (2012). Mesenchymal stem cells in tumor development: emerging roles and concepts. Cell Adhes. Migr. *6*, 220–230.

Dedeurwaerder, S., Desmedt, C., Calonne, E., Singhal, S.K., Haibe-Kains, B., Defrance, M., Michiels, S., Volkmar, M., Deplus, R., Luciani, J., et al. (2011). DNA methylation profiling reveals a predominant immune component in breast cancers. EMBO Mol Med *3*, 726–741.

Dorado, J., Lonardo, E., Miranda-Lorenzo, I., and Heeschen, C. (2011). Pancreatic cancer stem cells: new insights and perspectives. J. Gastroenterol. *46*, 966–973.

Drews-Elger, K., Brinkman, J.A., Miller, P., Shah, S.H., Harrell, J.C., da Silva, T.G., Ao, Z., Schlater, A., Azzam, D.J., Diehl, K., et al. (2014). Primary breast tumor-derived cellular models: characterization of tumorigenic, metastatic, and cancer-associated fibroblasts in dissociated tumor (DT) cultures. Breast Cancer Res. Treat. *144*, 503–517.

El-Haibi, C.P., Bell, G.W., Zhang, J., Collmann, A.Y., Wood, D., Scherber, C.M., Csizmadia, E., Mariani, O., Zhu, C., Campagne, A., et al. (2012). Critical role for lysyl oxidase in mesenchymal stem cell-driven breast cancer malignancy. Proc. Natl. Acad. Sci. USA *109*, 17460–17465.

Farazi, T.A., Horlings, H.M., Ten Hoeve, J.J., Mihailovic, A., Halfwerk, H., Morozov, P., Brown, M., Hafner, M., Reyal, F., van Kouwenhove, M., et al. (2011). MicroRNA sequence and expression analysis in breast tumors by deep sequencing. Cancer Res. *71*, 4443–4453.

Feber, A., Xi, L., Pennathur, A., Gooding, W.E., Bandla, S., Wu, M., Luketich, J.D., Godfrey, T.E., and Litle, V.R. (2011). MicroRNA prognostic signature for nodal metastases and survival in esophageal adenocarcinoma. Ann. Thorac. Surg. *91*, 1523–1530.

Fisher, S.E., and Scharff, C. (2009). FOXP2 as a molecular window into speech and language. Trends Genet. *25*, 166–177.

Ginestier, C., Hur, M.H., Charafe-Jauffret, E., Monville, F., Dutcher, J., Brown, M., Jacquemier, J., Viens, P., Kleer, C.G., Liu, S., et al. (2007). ALDH1 is a marker of normal and malignant human mammary stem cells and a predictor of poor clinical outcome. Cell Stem Cell *1*, 555–567.

Goldstein, R.H., Reagan, M.R., Anderson, K., Kaplan, D.L., and Rosenblatt, M. (2010). Human bone marrow-derived MSCs can home to orthotopic breast cancer tumors and promote bone metastasis. Cancer Res. *70*, 10044–10050.

Hanson, S.E., Kim, J., and Hematti, P. (2013). Comparative analysis of adipose-derived mesenchymal stem cells isolated from abdominal and breast tissue. Aesthet. Surg. J. *33*, 888–898.

Hu, Y., and Smyth, G.K. (2009). ELDA: extreme limiting dilution analysis for comparing depleted and enriched populations in stem cell and other assays. J. Immunol. Methods *347*, 70–78.

Hu, M., Yao, J., Carroll, D.K., Weremowicz, S., Chen, H., Carrasco, D., Richardson, A., Violette, S., Nikolskaya, T., Nikolsky, Y., et al. (2008). Regulation of in situ to invasive breast carcinoma transition. Cancer Cell *13*, 394–406.

Iorio, M.V., Visone, R., Di Leva, G., Donati, V., Petrocca, F., Casalini, P., Taccioli, C., Volinia, S., Liu, C.G., Alder, H., et al. (2007). MicroRNA signatures in human ovarian cancer. Cancer Res. *67*, 8699–8707.

Jung, Y., Kim, J.K., Shiozawa, Y., Wang, J., Mishra, A., Joseph, J., Berry, J.E., McGee, S., Lee, E., Sun, H., et al. (2013). Recruitment of mesenchymal stem cells into prostate tumours promotes metastasis. Nat Commun *4*, 1795.

Karnoub, A.E., Dash, A.B., Vo, A.P., Sullivan, A., Brooks, M.W., Bell, G.W., Richardson, A.L., Polyak, K., Tubo, R., and Weinberg, R.A. (2007). Mesenchymal stem cells within tumour stroma promote breast cancer metastasis. Nature *449*, 557–563.

Konopka, G., Bomar, J.M., Winden, K., Coppola, G., Jonsson, Z.O., Gao, F., Peng, S., Preuss, T.M., Wohlschlegel, J.A., and Geschwind, D.H. (2009). Human-specific transcriptional regulation of CNS development genes by FOXP2. Nature *462*, 213–217.

Li, S., Weidenfeld, J., and Morrisey, E.E. (2004). Transcriptional and DNA binding activity of the Foxp1/2/4 family is modulated by heterotypic and homotypic protein interactions. Mol. Cell. Biol. *24*, 809–822.

Liu, M., Casimiro, M.C., Wang, C., Shirley, L.A., Jiao, X., Katiyar, S., Ju, X., Li, Z., Yu, Z., Zhou, J., et al. (2009). p21CIP1 attenuates Ras- and c-Myc-dependent breast tumor epithelial mesenchymal transition and cancer stem cell-like gene expression in vivo. Proc. Natl. Acad. Sci. USA *106*, 19035–19039.

Liu, S., Ginestier, C., Ou, S.J., Clouthier, S.G., Patel, S.H., Monville, F., Korkaya, H., Heath, A., Dutcher, J., Kleer, C.G., et al. (2011). Breast cancer stem cells are regulated by mesenchymal stem cells through cytokine networks. Cancer Res. *71*, 614–624.

Ma, L., Teruya-Feldstein, J., and Weinberg, R.A. (2007). Tumour invasion and metastasis initiated by microRNA-10b in breast cancer. Nature *449*, 682–688.

Malanchi, I., Santamaria-Martínez, A., Susanto, E., Peng, H., Lehr, H.A., Delaloye, J.F., and Huelsken, J. (2012). Interactions between cancer stem cells and their niche govern metastatic colonization. Nature *481*, 85–89.

Mascaux, C., Laes, J.F., Anthoine, G., Haller, A., Ninane, V., Burny, A., and Sculier, J.P. (2009). Evolution of microRNA expression during human bronchial squamous carcinogenesis. Eur. Respir. J. *33*, 352–359.

McLean, K., Gong, Y., Choi, Y., Deng, N., Yang, K., Bai, S., Cabrera, L., Keller, E., McCauley, L., Cho, K.R., and Buckanovich, R.J. (2011). Human ovarian carcinoma–associated mesenchymal stem cells regulate cancer stem cells and tumorigenesis via altered BMP production. J. Clin. Invest. *121*, 3206–3219.

Miller, L.D., Smeds, J., George, J., Vega, V.B., Vergara, L., Ploner, A., Pawitan, Y., Hall, P., Klaar, S., Liu, E.T., and Bergh, J. (2005). An expression signature for p53 status in human breast cancer predicts mutation status, transcriptional effects, and patient survival. Proc. Natl. Acad. Sci. USA, *102*, 13550–13555.

Miyoshi, N., Ishii, H., Nagano, H., Haraguchi, N., Dewi, D.L., Kano, Y., Nishikawa, S., Tanemura, M., Mimori, K., Tanaka, F., et al. (2011). Reprogramming of mouse and human cells to pluripotency using mature microRNAs. Cell Stem Cell *8*, 633–638.

Myatt, S.S., and Lam, E.W. (2007). The emerging roles of forkhead box (Fox) proteins in cancer. Nat. Rev. Cancer *7*, 847–859.

Nair, R., Roden, D.L., Teo, W.S., McFarland, A., Junankar, S., Ye, S., Nguyen, A., Yang, J., Nikolic, I., Hui, M., et al. (2014). c-Myc and Her2 cooperate to drive a stem-like phenotype with poor prognosis in breast cancer. Oncogene *33*, 3992–4002.

Okamoto, O.K., Oba-Shinjo, S.M., Lopes, L., and Nagahashi Marie, S.K. (2007). Expression of HOXC9 and E2F2 are up-regulated in CD133(+) cells isolated from human astrocytomas and associate with transformation of human astrocytes. Biochim. Biophys. Acta *1769*, 437–442.

Pawitan, Y., Bjöhle, J., Amler, L., Borg, A.L., Egyhazi, S., Hall, P., Han, X., Holmberg, L., Huang, F., Klaar, S., et al. (2005). Gene expression profiling spares early breast cancer patients from adjuvant therapy: derived and validated in two population-based cohorts. Breast Cancer Res. *7*, R953–R964.

Pencheva, N., Tran, H., Buss, C., Huh, D., Drobnjak, M., Busam, K., and Tavazoie, S.F. (2012). Convergent multi-miRNA targeting of ApoE drives LRP1/LRP8-dependent melanoma metastasis and angiogenesis. Cell *151*, 1068–1082.

Polyak, K., and Weinberg, R.A. (2009). Transitions between epithelial and mesenchymal states: acquisition of malignant and stem cell traits. Nat. Rev. Cancer *9*, 265–273.

Prantl, L., Muehlberg, F., Navone, N.M., Song, Y.H., Vykoukal, J., Logothetis, C.J., and Alt, E.U. (2010). Adipose tissue-derived stem cells promote prostate tumor growth. Prostate *70*, 1709–1715.

Prockop, D.J., Kota, D.J., Bazhanov, N., and Reger, R.L. (2010). Evolving paradigms for repair of tissues by adult stem/progenitor cells (MSCs). J. Cell. Mol. Med. *14*, 2190–2199.

Quail, D.F., and Joyce, J.A. (2013). Microenvironmental regulation of tumor progression and metastasis. Nat. Med. *19*, 1423–1437.

Sabatier, R., Finetti, P., Cervera, N., Lambaudie, E., Esterni, B., Mamessier, E., Tallet, A., Chabannon, C., Extra, J.M., Jacquemier, J., et al. (2011). A gene expression signature identifies two prognostic subgroups of basal breast cancer. Breast Cancer Res. Treat. *126*, 407–420.

Sakurai, K., Furukawa, C., Haraguchi, T., Inada, K., Shiogama, K., Tagawa, T., Fujita, S., Ueno, Y., Ogata, A., Ito, M., et al. (2011). MicroRNAs miR-199a-5p and -3p target the Brm subunit of SWI/SNF to generate a double-negative feedback loop in a variety of human cancers. Cancer Res. *71*, 1680–1689.

Scapoli, L., Palmieri, A., Lo Muzio, L., Pezzetti, F., Rubini, C., Girardi, A., Farinella, F., Mazzotta, M., and Carinci, F. (2010). MicroRNA expression profiling of oral carcinoma identifies new markers of tumor progression. Int. J. Immunopathol. Pharmacol. *23*, 1229–1234.

Schwarzenbach, H., Milde-Langosch, K., Steinbach, B., Müller, V., and Pantel, K. (2012). Diagnostic potential of PTEN-targeting miR-214 in the blood of breast cancer patients. Breast Cancer Res. Treat. *134*, 933–941.

Shinagawa, K., Kitadai, Y., Tanaka, M., Sumida, T., Kodama, M., Higashi, Y., Tanaka, S., Yasui, W., and Chayama, K. (2010). Mesenchymal stem cells enhance growth and metastasis of colon cancer. Int. J. Cancer *127*, 2323–2333.

Shu, W., Yang, H., Zhang, L., Lu, M.M., and Morrisey, E.E. (2001). Characterization of a new subfamily of winged-helix/forkhead (Fox) genes that are expressed in the lung and act as transcriptional repressors. J. Biol. Chem. *276*, 27488–27497.

Shu, W., Lu, M.M., Zhang, Y., Tucker, P.W., Zhou, D., and Morrisey, E.E. (2007). Foxp2 and Foxp1 cooperatively regulate lung and esophagus development. Development *134*, 1991–2000.

Spiteri, E., Konopka, G., Coppola, G., Bomar, J., Oldham, M., Ou, J., Vernes, S.C., Fisher, S.E., Ren, B., and Geschwind, D.H. (2007). Identification of the transcriptional targets of FOXP2, a gene linked to speech and language, in developing human brain. Am. J. Hum. Genet. *81*, 1144–1157.

Suzuki, K., Sun, R., Origuchi, M., Kanehira, M., Takahata, T., Itoh, J., Umezawa, A., Kijima, H., Fukuda, S., and Saijo, Y. (2011). Mesenchymal stromal cells promote tumor growth through the enhancement of neovascularization. Mol. Med. *17*, 579–587.

Tavazoie, S.F., Alarcón, C., Oskarsson, T., Padua, D., Wang, Q., Bos, P.D., Gerald, W.L., and Massagué, J. (2008). Endogenous human microRNAs that suppress breast cancer metastasis. Nature *451*, 147–152.

Toullec, A., Gerald, D., Despouy, G., Bourachot, B., Cardon, M., Lefort, S., Richardson, M., Rigaill, G., Parrini, M.C., Lucchesi, C., et al. (2010). Oxidative stress promotes myofibroblast differentiation and tumour spreading. EMBO Mol Med *2*, 211–230.

Tsui, D., Vessey, J.P., Tomita, H., Kaplan, D.R., and Miller, F.D. (2013). FoxP2 regulates neurogenesis during embryonic cortical development. J. Neurosci. *33*, 244–258.

van de Vijver, M.J., He, Y.D., van't Veer, L.J., Dai, H., Hart, A.A., Voskuil, D.W., Schreiber, G.J., Peterse, J.L., Roberts, C., et al. (2002). A gene-expression signature as a predictor of survival in breast cancer. N. Engl. J. Med. *347*, 1999–2009.

Vernes, S.C., Oliver, P.L., Spiteri, E., Lockstone, H.E., Puliyadi, R., Taylor, J.M., Ho, J., Mombereau, C., Brewer, A., Lowy, E., et al. (2011). Foxp2 regulates gene networks implicated in neurite outgrowth in the developing brain. PLoS Genet. *7*, e1002145.

Volinia, S., Galasso, M., Sana, M.E., Wise, T.F., Palatini, J., Huebner, K., and Croce, C.M. (2012). Breast cancer signatures for invasiveness and prognosis defined by deep sequencing of microRNA. Proc. Natl. Acad. Sci. USA *109*, 3024–3029.

Wan, D., He, S., Xie, B., Xu, G., Gu, W., Shen, C., Hu, Y., Wang, X., Zhi, Q., and Wang, L. (2013). Aberrant expression of miR-199a-3p and its clinical significance in colorectal cancers. Med. Oncol. *30*, 378.

Yan, X.L., Fu, C.J., Chen, L., Qin, J.H., Zeng, Q., Yuan, H.F., Nan, X., Chen, H.X., Zhou, J.N., Lin, Y.L., et al. (2012). Mesenchymal stem cells from primary breast cancer tissue promote cancer proliferation and enhance mammosphere formation partially via EGF/EGFR/Akt pathway. Breast Cancer Res. Treat. *132*, 153–164.

Yang, H., Kong, W., He, L., Zhao, J.J., O'Donnell, J.D., Wang, J., Wenham, R.M., Coppola, D., Kruk, P.A., Nicosia, S.V., and Cheng, J.Q. (2008). MicroRNA expression profiling in human ovarian cancer: miR-214 induces cell survival and cisplatin resistance by targeting PTEN. Cancer Res. *68*, 425–433.

Zhang, Y., Goss, A.M., Cohen, E.D., Kadzik, R., Lepore, J.J., Muthukumaraswamy, K., Yang, J., DeMayo, F.J., Whitsett, J.A., Parmacek, M.S., and Morrisey, E.E. (2008). A Gata6-Wnt pathway required for epithelial stem cell development and airway regeneration. Nat. Genet. *40*, 862–870.

Zhang, X.J., Ye, H., Zeng, C.W., He, B., Zhang, H., and Chen, Y.Q. (2010). Dysregulation of miR-15a and miR-214 in human pancreatic cancer. J Hematol Oncol *3*, 46.

Zhou, J., Ng, S.B., and Chng, W.J. (2013). LIN28/LIN28B: an emerging oncogenic driver in cancer stem cells. Int. J. Biochem. Cell Biol. *45*, 973–978.